Coherence attribute at different spectral scales

Fangyu Li[1] and Wenkai Lu[2]

Abstract

In general, we wish to interpret the most broadband data possible. However, broadband data do not always provide the best insight for seismic attribute analysis. Obviously, spectral bands contaminated by noise should be eliminated. However, tuning gives rise to spectral bands with higher signal-to-noise ratios. To quantify geologic discontinuities in different scales, we combined spectral decomposition and coherence. Using spectral decomposition, the spectral amplitudes corresponding to a given scale geologic discontinuity, as well as some subtle features, which would otherwise be buried within the broadband seismic response, can be extracted. We applied this workflow to a 3D land data volume acquired over the Tarim Basin, Northwest China, where karst forms the principle reservoirs. We found that channels are better illuminated around 18 Hz, while subtle discontinuities were better delineated around 25 Hz.

Introduction

Structural and stratigraphic discontinuities such as channels, faults and fractures may provide lateral variation in seismic expression. Seismic attributes such as coherence delineate such lateral discontinuities, accelerate interpretation, and provide images of subtle features that may otherwise have been overlooked. Al-Dossary and Marfurt (2006) use both long- and short-wavelength curvature attributes from multispectral curvature estimation to enhance geologic features having different scales. Sun et al. (2010) use discrete frequency coherence cubes in fracture detection and find that high-frequency components can provide greater detail. Gao (2013) notices that more subtle structural details in reservoirs are revealed using a higher frequency wavelet as the spectral probe.

The seismic response of a given geologic feature is expressed differently at different spectral bands. Often, a particular frequency component carries the information regarding structure and stratigraphy. Spectral decomposition methods map 1D signal into the 2D time and frequency plane, generating amplitude and phase spectral components (Partyka et al., 1999; Castagna et al., 2003). Extracting the spectral components at different dominant frequencies may provide more precise perspectives of given geologic structures. For example, the thickness of a channel and its spectral amplitude are strongly correlated (Laughlin et al., 2002).

Time-frequency representation can be broadly divided into two classes: linear time-frequency and bilinear (quadratic) time-frequency transforms. Chakraborty and Okaya (1995) and Partyka et al. (1999) compute seismic spectral response using the short-time Fourier transform (STFT). Since then, other linear time-frequency transforms, such as the continuous wavelet transform (Sinha et al., 2005) and the S transform (Matos et al., 2005) as well as bilinear time-frequency transforms, such as the smoothed pseudo-Wigner-Ville distribution (Li and Zheng, 2008) have been introduced to improve the temporal data analysis and frequency resolution. Fourier transform representation of the convolution between the signal and the time-frequency atom is equivalent to a suite of narrow band-pass filters, resulting in a suite of complex spectra (Qian, 2002). In contrast, bilinear transforms based on quadratic energy do not generate phase information. Spectral magnitude of the joint time-frequency spectrum is routinely used in reservoir characterization (Liu and Marfurt, 2007), hydrocarbon detection (Castagna et al., 2003; Lu and Li, 2013), and measuring tuning and attenuation effects (Partyka et al., 1999). However, to delineate lateral stratigraphic discontinuities (Matos et al., 2011), we need the spectral phase component of the joint time-frequency distribution. Fahmy et al. (2005) apply a band-pass filter using the most significant frequency bandwidth of seismic data for reservoir illumination. Hardage (2009) demonstrates that frequency-constrained seismic data can provide improved images of geologic systems.

[1]Formerly Tsinghua University, Department of Automation, Beijing, China; presently The University of Oklahoma, ConocoPhillips School of Geology and Geophysics, Norman, Oklahoma, USA. E-mail: fangyu.li@ou.edu.
[2]Tsinghua University, State Key Laboratory of Intelligent Technology and Systems, Tsinghua National Laboratory for Information Science and Technology, Department of Automation, Beijing, China. E-mail: lwkmf@mail.tsinghua.edu.cn.

Manuscript received by the Editor 18 June 2013; revised manuscript received 19 October 2013. This paper appears in *Interpretation*, Vol. 2, No. 1 (February 2014); p. 1–8, 10 FIGS.
http://dx.doi.org/10.1190/INT-2013-0089.1.

Estimates of seismic coherence (Bahorich and Farmer, 1995; Marfurt et al., 1998; Gerstzenkorn and Marfurt, 1999; Lu et al., 2005) measure changes in waveform and provide a quantitative measure of geologic discontinuities. In general, most interpreters apply coherence to the final processed, broadbanded data (Chopra and Marfurt, 2007). Coherence can be computed from the real seismic or from the analytic seismic data (Taner et al., 1979). Using the analytic trace can sharpen discontinuities (Guo et al., 2009). For this reason, we adopt linear rather than quadratic time-frequency analysis methods to generate complex spectra in our work.

In this paper, we combine spectral decomposition, which extracts complex spectral amplitudes from the frequency bands of interest, and complex coherence computation to map discontinuities at different vertical

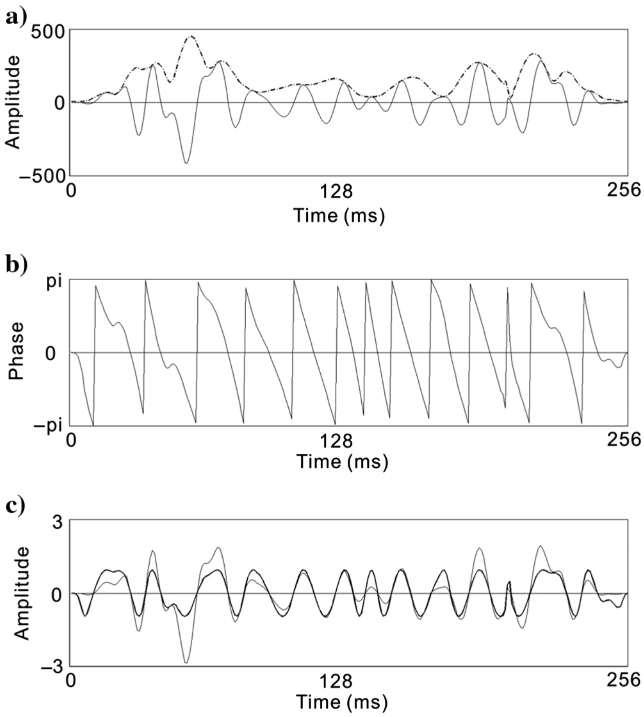

Figure 1. A seismic trace and its derived attributes: (a) the measured seismic trace (solid line) and the instantaneous envelope (dotted line), (b) instantaneous phase, and (c) a scaled version of the measured seismic trace (light line) and the cosine of the instantaneous phase (heavy line).

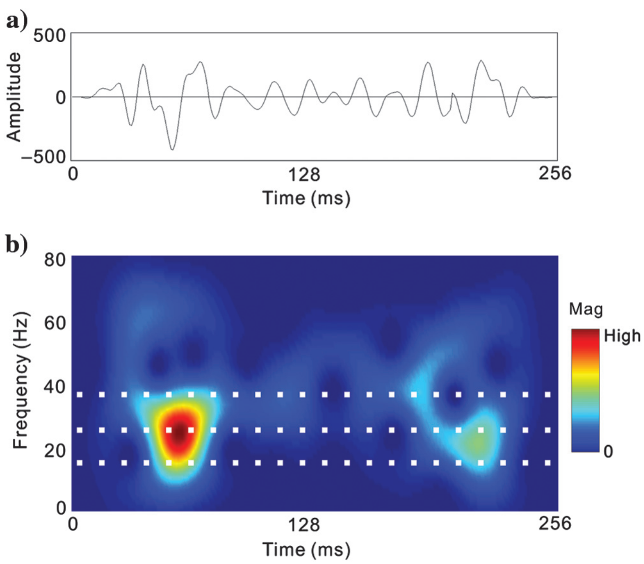

Figure 2. (a) A seismic trace and (b) its STFT spectrogram. The white dotted lines indicate the positions of the extracted isofrequency spectral components at 18, 25, and 38 Hz.

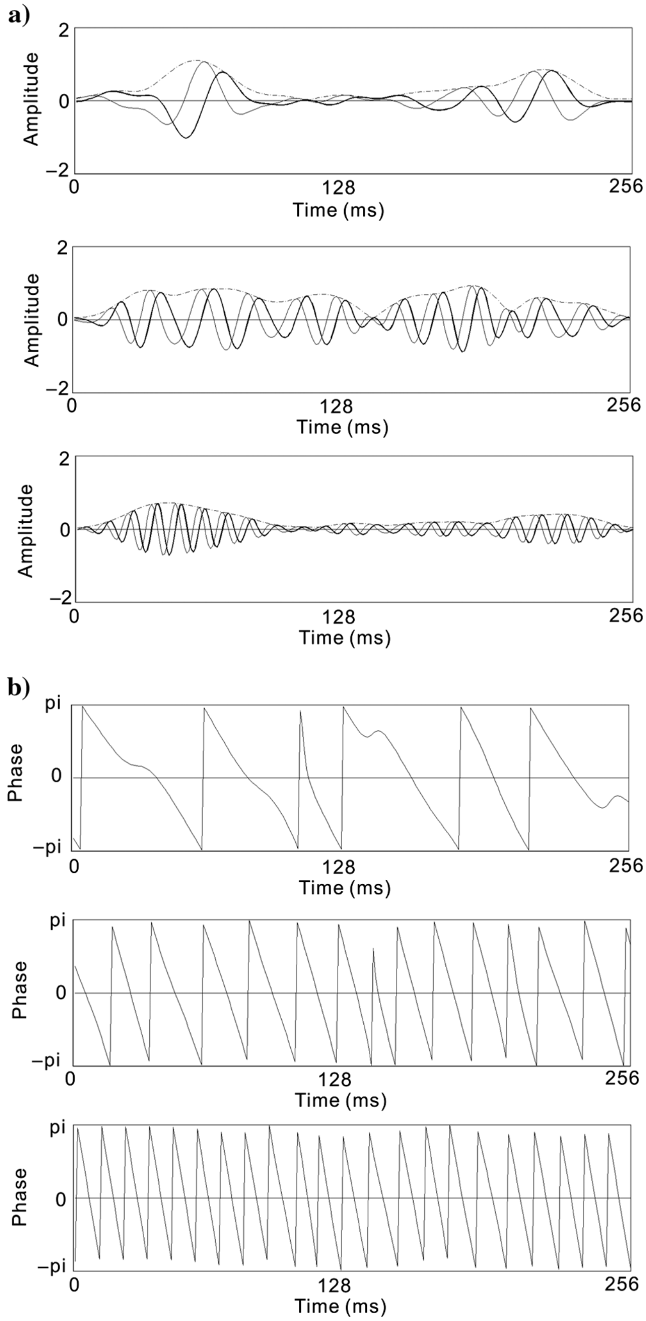

Figure 3. (a) Real (heavy line) and imaginary (light line) components and envelope (dotted line) at 18, 25, and 38 Hz. (b) Corresponding instantaneous phase components.

scales. We begin our paper with a review of complex spectra and coherence. Then, we propose a workflow of complex spectral coherence calculation. Finally, we apply the proposed workflow on fault delineation and channel detection, and obtain promising results.

Complex spectra and coherence

Complex seismic trace analysis has long been used to aid seismic interpretation (Taner et al., 1979; Barnes, 2007). Traditional complex signal analysis is based on the Hilbert transform. The original data and their Hilbert transform that satisfies the Cauchy-Riemann integral condition form an analytic signal (Claerbout, 1976). Complex trace analysis represents the measured signal as the product of two independent and separable functions: instantaneous envelope $e(t) = \|c(t)\|$ and the cosine of the instantaneous phase $\theta(t)$ as

$$c(t) = e(t)\cos[\theta(t)] + ie(t)\sin[\theta(t)]. \tag{1}$$

Figure 1 shows a seismic trace and its derived complex attributes. Figure 2 displays the seismic trace shown in Figure 1 and its spectrogram (magnitude of the STFT). The magnitude component characterizes variations of the seismic response such as attenuation, which can be caused by reservoir and hydrocarbon accumulation. We extract three isofrequency components from the spectrum, at 18, 25, and 38 Hz, indicated by the white dotted lines in Figure 2b, and we display them as the dashed lines in Figure 3. The real and imaginary components of the data are displayed as thin and bold solid lines in Figure 3a, while the phase components are plotted in Figure 3b. The spectral components are a function of the signal and the Gaussian window used. Different carrier frequencies measure the seismic behavior at different scales. The magnitude component is sensitive to changes in impedance while the phase component is sensitive to stratigraphy. Subtle geologic features, which are usually buried in broadband data, can be detected on isofrequency components as

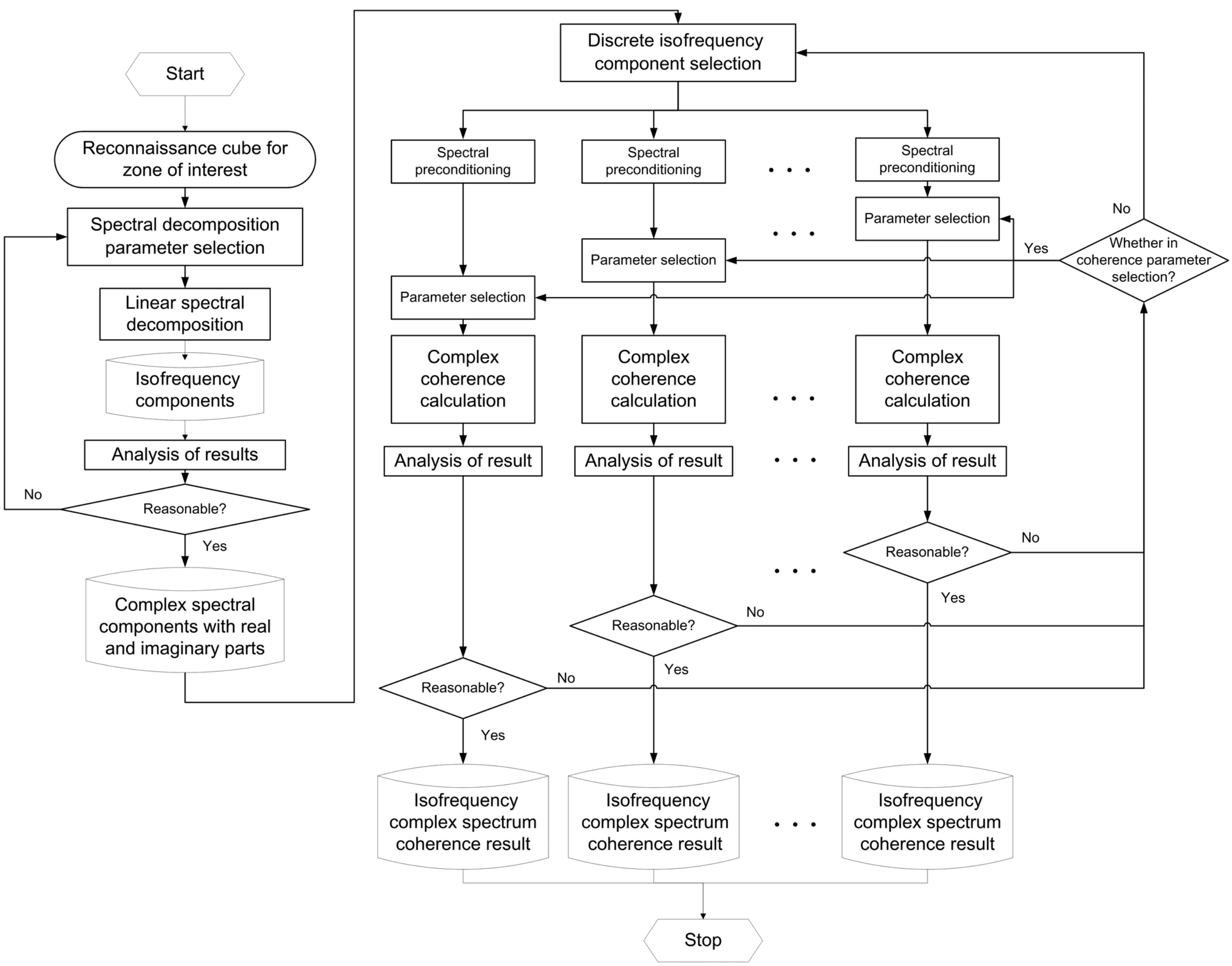

Figure 4. Workflow of complex spectral coherence attribute.

the disturbance when other frequencies have been suppressed.

In this work, we will apply coherence to measure the similarity of complex spectral components of the seismic data. Coherence has several implementations: crosscorrelation-based coherence, semblance-based coherence, variance-based coherence, eigenstructure-based coherence, least-squares-based coherence, and gradient structure tensor-based coherence. Different measurements of seismic character variability have different sensitivities to geology, spectral bandwidth. and seismic noise. The size of the vertical and lateral analysis windows also produces different images such that no one coherence algorithm is always "best."

Here, we use an eigenstructure-based coherence algorithm. Traditionally, for the computation of what Gersztenkorn and Marfurt (1999) call "C3 coherence," a 3D analysis cube enclosing a relatively small subvolume of traces is selected. The analysis cube moves throughout the 3D seismic volume, and the full data covariance matrix is assembled by crosscorrelating the 3D analysis cube:

$$C_{kj} = \sum_{m=1}^{M} (d_{mk} * d_{mj}), \tag{2}$$

where C_{kj} is the kjth element of the covariance matrix $\mathbf{C}$, M is the sample number of the analysis cube, and d_{mk} and d_{mj} are the amplitudes of the mth sample of the kth and jth trace.

Computing covariance matrices from the complex components needs to include both imaginary and real components, giving

$$C_{kj} = \sum_{m=1}^{M} (\|d_{mk}\| \cos \varphi_{mk} * \|d_{mj}\| \cos \varphi_{mj} - \|d_{mk}\| \sin \varphi_{mk} * \|d_{mj}\| \sin \varphi_{mj}), \tag{3}$$

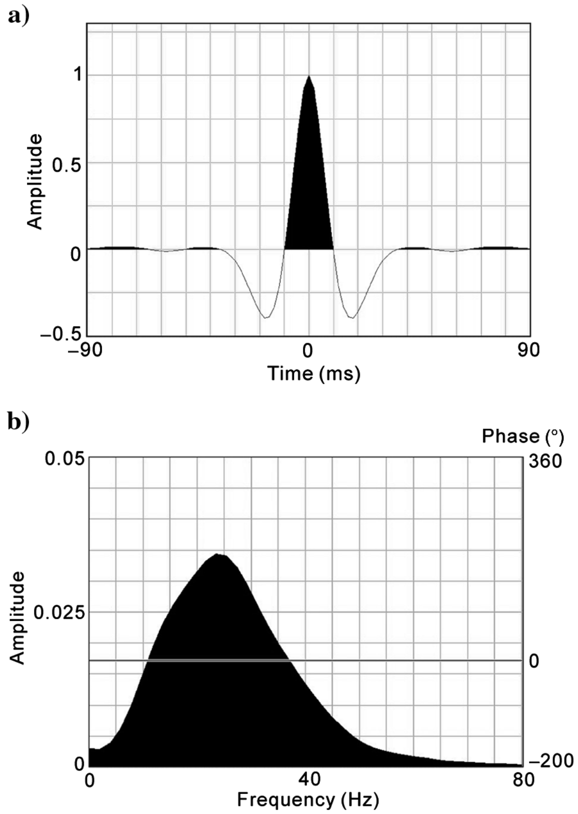

Figure 5. Waveform and spectrum of the wavelet extracted from the data set.

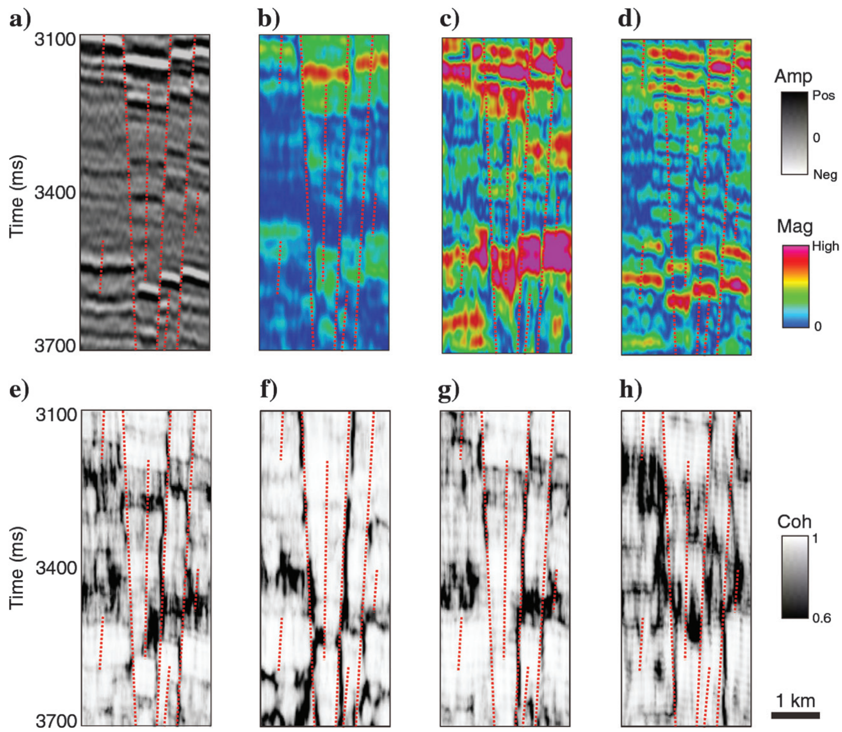

Figure 6. Fault detection by complex spectral coherence. Vertical slices through (a) seismic amplitude (b) 18, (c) 25, and (d) 38 Hz spectral magnitude components and (e) broadband, (f) 18, (g) 25, and (h) 38 Hz component coherence volumes. The dotted lines indicate faults. Vertical analysis window = ±20 ms. Horizontal analysis window = five traces.

where $\|d_{mn}\|$ is the magnitude, φ_{mn} is the phase of the complex spectral components, and $\|d_{mn}\| \sin \varphi_{mn}$ and $\|d_{mn}\| \cos \varphi_{mn}$ are the imaginary and real components, respectively. During 3D attribute computation, Gersztenkorn (2012) uses a similar way to facilitate the representation for matrix entries.

Application

The entire workflow of complex spectral coherence calculation is displayed in Figure 4. To obtain isofrequency components at different frequencies, these spectral components should be checked for both resolution and artifact suppression. Large windows may be more "stable," but they may mix stratigraphy. Small windows may be too small to contain a period of interest. After obtaining complex spectral components with both real and imaginary parts, the selected discrete isofrequency components are used as input to coherence. Because of thin bed tuning, some spectral components will illuminate geology better than others, as Fahmy et al. (2005) find with AVO analysis. Other components may be dominated by noise and should be rejected, as Hardage (2009) shows.

Figure 5 shows the waveform and the spectrum of the wavelet extracted from our well tie. This wavelet is zero phase, centered at about 25 Hz, so we will illustrate our analysis with 10, 25, and 40 Hz frequencies. In this application, we used STFT as the linear transform and the eigenstucture-based algorithm as the coherence attribute.

Fault Delineation

Figure 6 displays a fault detection example. Figure 6a shows seismic amplitude, Figure 6b–6d shows the corresponding vertical slices through 10, 25, and 40 Hz spectral magnitude components, while vertical slices through the coherence volumes from the original ("broadband") shown in Figure 6e and Figure 6f–6h are the 10, 25, and 40 Hz spectral component coherence profiles, respectively. Red dotted lines indicate normal faults. But, the broadband coherence result delineates the main fault on the right but not the one on the left. In contrast, the low-frequency spectral coherence delineates both main faults most clearly, while the middle- and high-frequency spectral coherence highlights smaller discontinuities near the faults that we interpret to be conjugate faults. The 10 Hz component of the coherence attribute shows more continuous images of large scale features.

Figure 7 displays more subtle discontinuities. Figure 7a shows seismic amplitude with corresponding 10 (Figure 7b), 25 (Figure 7c), and 40 Hz (Figure 7d) spectral magnitude components, while vertical slices are shown through the coherence volumes from

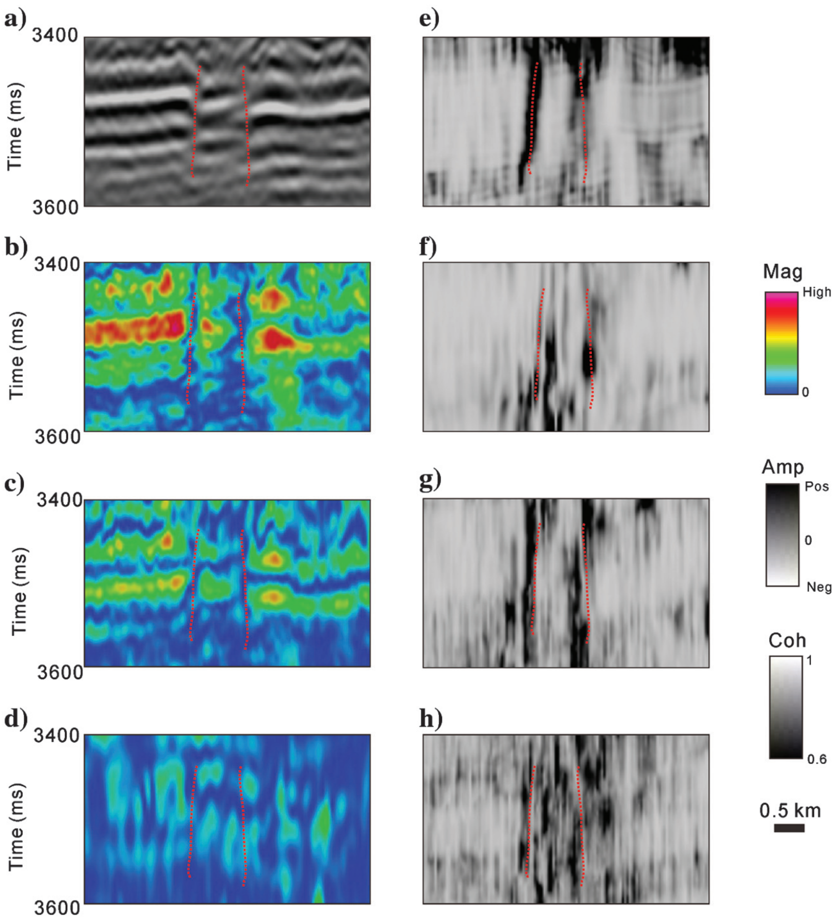

Figure 7. Subtle discontinuity delineation by complex spectral coherence. Vertical slices through (a) seismic amplitude, (b) 18, (c) 25, and (d) 38 Hz spectral magnitude components and (e) broadband, (f) 18, (g) 25, and (h) 38 Hz component coherence volumes. The dotted lines indicate the subtle discontinuity.

broadband (Figure 7e), 10 (Figure 7f), 25 (Figure 7g), and 40 Hz (Figure 7h) spectral components, respectively. The fracture lineaments in Figure 7g correlate with textures with faulting we expect to occur with compression.

Channel delineation

Before the calculation of complex spectral coherence, we analyzed the frequency components on the target horizon, shown in Figure 8. Different types of geologic structures with different scales reveal different peak frequencies. Seismic data analysis of stronger frequency bandwidths improves the delineation of certain geologic structures. Figure 9 displays horizontal slices from different component coherence results. Figure 9a shows the broadband result, while Figure 9b–9d shows the 18, 25, and 38 Hz components, respectively. The channels indicated by the left dotted ellipse are better illuminated on the 18 Hz spectral component. The channels indicated by the right dotted ellipse are better illuminated by the 18 Hz spectral component in the upper and middle parts, but in the bottom part by the 25 Hz component. The faults are better seen in the broadband volume.

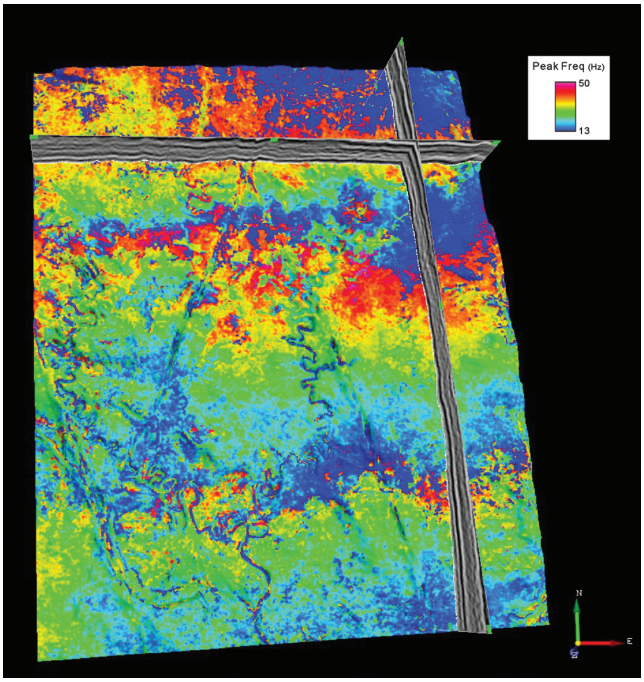

Figure 8. Peak frequency image of the target horizon.

For easier comparison and viewing more detailed features, we integrated the horizontal slices of different complex spectral coherence into a color-blended image displayed in Figure 10 (such as is done for enhanced understanding of temporal location of depositional and structural elements by Leppard et al. (2010)). In Figure 10, the 10, 25, and 38 Hz spectral components paint red, green, and blue (RGB), respectively. As shown in the RGB color map, if the energies in three color channels are equal, the blended color is white, and if the energy of one channel is stronger than the other two, its color would dominate. We can find a lot of new information shown by the color changes. As there is a strong correlation between channel thickness and the spectral decomposition component, different scale channels correspond to different frequency bands, and they will show up in different colors. For example, we can still remember the channel in the right dotted ellipse in Figure 9, and its boundaries are clearer on the 18 Hz spectral coherence, which is the red component in the color-blended image. Because the coherence values at the edges of channels are low, it appears as light blue after blending, which is the opposite color of red. So, the low coherence at low frequency indicates that the channel is fairly thick. In the same way, we can use this pattern to recognize the thickness of channels.

The examples above demonstrate that the proposed workflow can highlight the different scale faults,

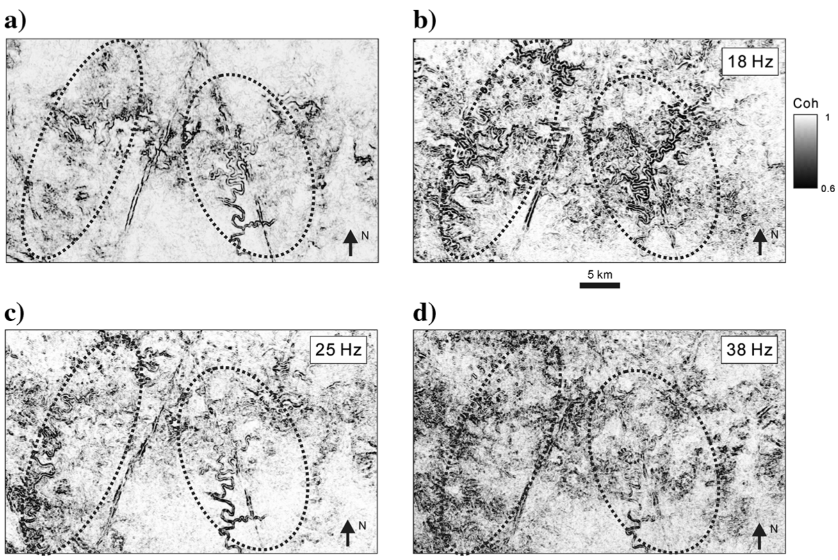

Figure 9. Channel detection by complex spectral coherence. Horizontal slices through (a) broadband, (b) 18, (c) 25, and (d) 38 Hz component coherence volumes. Dotted circles indicate two channel systems.

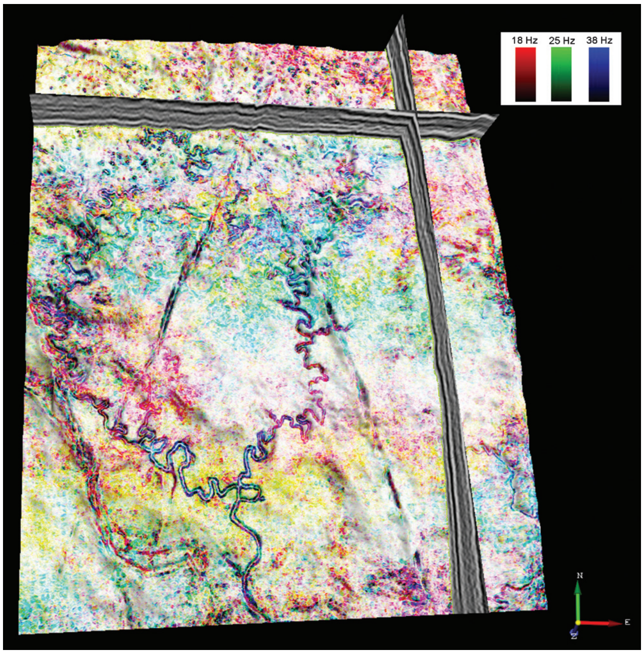

Figure 10. Color-blended images. Integration of complex spectral coherence attributes: 18, 25, and 38 Hz components paint red, green, and blue, respectively.

fractures, and channels within a certain frequency bandwidth. Conversely, we can also identify and quantify the scale of discontinuities through the comparison between the serial complex spectral coherence attributes.

Conclusions

We propose a workflow for identification and accurate estimation of geologic discontinuity at different temporal scales. Our approach is based on a linear time-frequency transform and complex coherence calculation, and it is shown to be valuable for prediction of discontinuity lineaments in deformed strata. Interpreters can choose their own combinations of linear spectral decomposition method and coherence algorithm to suit their needs. The application of complex spectral coherence shows that it is useful for detecting different-scale structural and stratigraphic discontinuity features.

Acknowledgments

This work is supported by the China State Key Science and Technology Project on Marine Carbonate Reservoir Characterization (2011ZX05004-003). We thank Petro-China for permission to use their data in this research. The final version of this paper benefited tremendously from the comments and suggestions of K. J. Marfurt. We give special thanks to him. Finally, we thank the associate editor of *Interpretation* and two reviewers.

References

Al-Dossary, S., and K. J. Marfurt, 2006, 3-D volumetric multispectral estimates of reflector curvature and rotation: Geophysics, **71**, no. 5, P41–P51, doi: 10.1190/1.2242449.

Bahorich, M. S., and S. L. Farmer, 1995, 3-D seismic coherence for faults and stratigraphic features: The Leading Edge, **14**, 1053–1058, doi: 10.1190/1.1437077.

Barnes, A. E., 2007, A tutorial on complex seismic trace analysis: Geophysics, **72**, no. 6, W33–W43, doi: 10.1190/1.2785048.

Castagna, J., S. Sun, and R. Siegfried, 2003, Instantaneous spectral analysis: Detection of low-frequency shadows associated with hydrocarbons: The Leading Edge, **22**, 120–127, doi: 10.1190/1.1559038.

Chakraborty, A., and D. Okaya, 1995, Frequency-time decomposition of seismic data using wavelet based methods: Geophysics, **60**, 1906–1916, doi: 10.1190/1.1443922.

Chopra, S., and K. J. Marfurt, 2007, Seismic attributes for prospect identification and reservoir characterization: SEG.

Claerbout, J. F., 1976, Fundamentals of geophysical data processing: McGraw-Hill.

Fahmy, W. A., G. Matteucci, D. Butters, and J. Zhang, 2005, Successful application of spectral decomposition technology toward drilling of a key offshore development well: 75th Annual International Meeting, SEG, Expanded Abstracts, 262–264.

Gao, D., 2013, Wavelet spectral probe for seismic structure interpretation and fracture characterization: A workflow with case studies: Geophysics, **78**, no. 5, O57–O67, doi: 10.1190/geo2012-0427.1.

Gersztenkorn, A., 2012, A new approach for detecting topographic and geologic information in seismic data: Geophysics, **77**, no. 2, V81–V90, doi: 10.1190/geo2011-0216.1.

Gersztenkorn, A., and K. J. Marfurt, 1999, Eigenstructure based coherence computations: As an aid to 3-D structural and stratigraphic mapping: Geophysics, **64**, 1468–1479, doi: 10.1190/1.1444651.

Guo, H., K. J. Marfurt, and J. Liu, 2009, Principal component spectral analysis: Geophysics, **74**, no. 4, P35–P43, doi: 10.1190/1.3119264.

Hardage, B., 2009, Frequencies are fault finding factors: Looking low aids data interpretation: AAPG Explorer, **30**, no. 9, 34.

Laughlin, K., P. Garossino, and G. Partyka, 2002, Spectral decomposition applied to 3D: AAPG Explorer, **23**, 28–31.

Leppard, C., A. Eckersly, and S. Purves, 2010, Quantifying the temporal and spatial extent of depositional and structural elements in 3D seismic data using spectral decomposition and multi attribute RGB blending, *in* L. J. Wood, T. T. Simo, and N. C. Rosen, eds., Seismic imaging of depositional and geomorphic systems: 30th Annual GCSSEPM Foundation Bob F. Perkins Research Conference: GCSSEPM, 1–10.

Li, Y. D., and X. D. Zheng, 2008, Spectral decomposition using Wigner-Ville distribution with applications to carbonate reservoir characterization: The Leading Edge, **27**, 1050–1057, doi: 10.1190/1.2967559.

Liu, J., and K. J. Marfurt, 2007, Instantaneous spectral attributes to detect channels: Geophysics, **72**, no. 2, P23–P31, doi: 10.1190/1.2428268.

Lu, W. K., and F. Y. Li, 2013, Seismic spectral decomposition using deconvolutive short time Fourier transform spectrogram: Geophysics, **78**, no. 2, V43–V51, doi: 10.1190/geo2012-0125.1.

Lu, W. K., Y. D. Li, S. W. Zhang, H. Q. Xiao, and Y. D. Li, 2005, Higher-order statistics and super-trace based coherence estimation algorithm: Geophysics, **70**, no. 3, P13–P18, doi: 10.1190/1.1925746.

Marfurt, K. J., R. L. Kirlin, S. L. Farmer, and M. S. Bahorich, 1998, 3-D seismic attributes using a semblance-based coherency algorithm: Geophysics, **63**, 1150–1165.

Matos, M. C., O. Davogustto, and K. Zhang, 2011, Detecting stratigraphic discontinuities using time-frequency seismic phase residues: Geophysics, **76**, no. 2, P1–P10, doi: 10.1190/1.3528758.

Matos, M. C., P. Osorio, E. C. Mundim, and M. Moraces, 2005, Characterization of thin beds through joint time-frequency analysis applied to a turbidite reservoir in Compos Basin, Brazil: 75th Annual International Meeting, SEG, Expanded Abstracts, 1429–1432.

Partyka, G. A., J. Gridley, and J. Lopez, 1999, Interpretational applications of spectral decomposition in reservoir characterization: The Leading Edge, **18**, 353–360, doi: 10.1190/1.1438295.

Qian, S., 2002, Introduction to time-frequency and wavelet transforms: Prentice Hall PTR.

Sinha, S., P. S. Routh, P. D. Anno, and J. P. Castagna, 2005, Spectral decomposition of seismic data with continuous-wavelet transform: Geophysics, **70**, no. 6, P19–P25, doi: 10.1190/1.2127113.

Sun, D. S., Y. Ling, X. Y. Guo, J. Gao, and J. X. Lin, 2010, Application of discrete frequency coherence cubes in the fracture detection of volcanic rocks in full-azimuth seismic data: 80th Annual International Meeting, SEG, Expanded Abstracts, 1342–1346.

Taner, M. T., F. Koehler, and R. E. Sheriff, 1979, Complex seismic trace analysis: Geophysics, **44**, 1041–1063, doi: 10.1190/1.1440994.

Fangyu Li received Bachelor's (2009) and Master's (2013) degrees in electrical engineering from Beihang University and Tsinghua University. He is pursuing a Ph.D. in geophysics at the University of Oklahoma. He is working on seismic attribute assisted interpretation, and his research interests include signal processing, spectral decomposition, geologic discontinuity detection, reservoir characterization, and seismic attenuation estimation.

Wenkai Lu is a professor at the department of automation, Tsinghua University. Lu received a Ph.D. (1996) in geophysics from China University of Petroleum (Beijing). His main research interests are seismic signal processing, seismic attributes analysis, signal and image processing. Lu is a member of SEG and EAGE.